Geophysical Journal International

Geophys. J. Int. (2015) **200,** 1267–1278
GJI Seismology

doi: 10.1093/gji/ggu460

Isotropic source terms of San Jacinto fault zone earthquakes based on waveform inversions with a generalized CAP method

Z. E. Ross,[1] Y. Ben-Zion[1] and L. Zhu[2]

[1] *Department of Earth Sciences, University of Southern California, Los Angeles, CA* 90089-0740, *USA. E-mail: zross@usc.edu*
[2] *Department of Earth and Atmospheric Sciences, Saint Louis University, St. Louis, MO* 63108, *USA*

Accepted 2014 December 1. Received 2014 November 28; in original form 2014 April 10

SUMMARY

We analyse source tensor properties of seven $M_w > 4.2$ earthquakes in the complex trifurcation area of the San Jacinto Fault Zone, CA, with a focus on isotropic radiation that may be produced by rock damage in the source volumes. The earthquake mechanisms are derived with generalized 'Cut and Paste' (gCAP) inversions of three-component waveforms typically recorded by >70 stations at regional distances. The gCAP method includes parameters ζ and χ representing, respectively, the relative strength of the isotropic and CLVD source terms. The possible errors in the isotropic and CLVD components due to station variability is quantified with bootstrap resampling for each event. The results indicate statistically significant explosive isotropic components for at least six of the events, corresponding to ~0.4–8 per cent of the total potency/moment of the sources. In contrast, the CLVD components for most events are not found to be statistically significant. Trade-off and correlation between the isotropic and CLVD components are studied using synthetic tests with realistic station configurations. The associated uncertainties are found to be generally smaller than the observed isotropic components. Two different tests with velocity model perturbation are conducted to quantify the uncertainty due to inaccuracies in the Green's functions. Applications of the Mann–Whitney *U* test indicate statistically significant explosive isotropic terms for most events consistent with brittle damage production at the source.

Key words: Fault zone rheology; Earthquake source observations; Seismic monitoring and test-ban treaty verification; Dynamics and mechanics of faulting.

1 INTRODUCTION

Typical inversions of seismic waveforms for earthquake source properties assume pure deviatoric deformation with no volume change in the source region. The main reason for this is the dominance of shear deformation during earthquake failures associated with elastic rebound around the source volume (e.g. Reid 1910). In addition, incorporation of small isotropic components in derivations of source tensors can lead to instabilities in the inversion process. A number of studies (Kawakatsu 1991, 1996; Hara *et al.* 1995; Dufumier & Rivera 1997) performed detailed analysis of the correlation structure of different source components and inherent resolution of the isotropic components. The results from these studies suggest that in many cases, including the isotropic component in the inversion makes the problem intractable. Therefore, routine derivations of earthquake mechanisms are often done with inversions that are constrained to produce pure double-couple (DC; or sometimes pure deviatoric) tensors (e.g. Hardebeck & Shearer 2002; Yang *et al.* 2012). Inversions that include isotropic components are typically limited to analyses of deep events (Kawakatsu 1991), explosions (Patton & Taylor 2011; Xu *et al.* 2012), and earthquakes in geothermal, volcanic and other areas with elevated fluid content (Dreger *et al.* 2000; Minson *et al.* 2007; Ma *et al.* 2012).

Standard inversions of seismic data for moment tensors (e.g. Backus & Mulcahy 1976a,b; Tape & Tape 2013) assume that the elastic moduli in the source volume are unchanged during the failure process. While this may hold for some cases such as deep seismic events, rock failure in the brittle lithosphere is accompanied by significant (transient) changes of elastic moduli (e.g. Lockner *et al.* 1977; Stanchits *et al.* 2006; Hamiel *et al.* 2009). The repeating occurrences of brittle failures in earthquake fault zones produce belts of damaged rocks (e.g. Dor *et al.* 2008; Wechsler *et al.* 2009; Mitchell *et al.* 2011) with seismic velocities that can be reduced by 30 per cent or more (e.g. Lewis *et al.* 2005; Yang *et al.* 2011; Allam & Ben-Zion 2012). The spatio-temporal variations of elastic moduli within and across earthquake rupture zones (and other regions sustaining brittle failure) motivates quantifying the sources of radiation with potency tensors that are based solely on the inelastic (transformational) strain in the source volumes (e.g. Ben-Zion 2003, 2008; Ampuero & Dahlen 2005; Chapman & Leaney 2012).

Ben-Zion and Ampuero (2009) derived a seismic representation theorem that includes, in addition to the classical inelastic strain

(and corresponding stress glut), coseismic changes of elastic moduli in the source volume. The dynamic changes of elastic moduli are predicted to produce generically 'damage-related-radiation' that can have an appreciable isotropic component. While the overall source may still be dominated by deviatoric deformation, a small isotropic component can lead to dynamic changes of normal stresses at the source region that can have significant effects on many aspects of earthquake physics (e.g. Brune *et al.* 1993; Ben-Zion 2001). It is therefore important to resolve the possible existence of (small) isotropic earthquake source terms.

Zhu & Ben-Zion (2013) provided decompositions of general (deviatoric plus isotropic) potency and moment source tensors that can be used efficiently in waveform inversions based on the Cut-and-Paste (CAP) method (Zhu & Helmberger 1996). A number of other source tensor decompositions have been proposed and used by various authors (e.g. Julian *et al.* 1998; Chapman & Leaney 2012; Tape & Tape 2013; Vavryčuk 2014). Different decompositions may be more suitable for different purposes and inversion schemes. In this paper, we use a generalized CAP (gCAP) algorithm based on the decomposition of Zhu & Ben-Zion (2013) to derive source tensor properties of seven $M_w > 4.2$ earthquakes. The analysed events occur in a geometrically complex region of the San Jacinto fault zone (SJFZ), and are therefore expected to produce damage-related-radiation with some isotropic source terms. Each solution is rigorously tested using a set of statistical techniques to quantify the uncertainty present in the inverse problem. The results indicate that small, but statistically robust, explosive isotropic components are likely present in at least six of the earthquakes examined.

2 METHODOLOGY AND RESULTS

Seismic sources can be described in the point-source approximation by a symmetric second-order tensor that can be decomposed into constant-volume (deviatoric) and volumetric (isotropic) terms (e.g. Aki & Richards 2002). This representation has many practical applications since the source tensor elements are linearly related to the generated ground motions. There are numerous algorithms for determining seismic source tensor properties with appropriate Green's functions, using various decompositions and inversion schemes. The most common decomposition parameterizes the source as the sum of DCs, compensated linear vector dipoles (CLVD) and isotropic (ISO) components (e.g. Julian *et al.* 1998). The choice of parameterization is non-unique, and is often done to provide bounds to individual source components that do not exist for the elements of the source tensor themselves. These bounds can be useful for both computational purposes as well as conceptual ones.

In this study, we use the source decomposition of Zhu & Ben-Zion (2013):

$$P_{ij} = \frac{P_0}{\sqrt{2}}\left(\frac{\zeta}{\sqrt{3}}\delta_{ij} + \sqrt{1-\zeta^2}D_{ij}\right), \tag{1a}$$

where P_{ij} is the seismic potency tensor (e.g. Ben-Zion 2003), P_0 is the scalar potency, δ_{ij} is the Kronecker delta and ζ is the isotropic parameter. The latter is defined by

$$\zeta = \sqrt{\frac{2}{3}}\frac{\mathrm{tr}(\mathbf{P})}{P_0}, \tag{1b}$$

and it varies from -1 for implosive sources to 1 for explosive sources. D_{ij} is a traceless tensor quantifying the deviatoric component of the source:

$$D_{ij} = \sqrt{1-\chi^2}D_{ij}^{\mathrm{DC}} + \chi D_{ij}^{\mathrm{CLVD}}, \tag{1c}$$

with χ representing the strength of the CLVD source and having a range of $[-1/2, 1/2]$. In (1c), D_{ij}^{DC} and D_{ij}^{CLVD} are normalized potency tensors for the DC and CVLD sources, respectively. The relative strengths of the individual components can be quantified (Zhu & Ben-Zion 2013) by

$$|\Lambda_{\mathrm{ISO}}| + |\Lambda_{\mathrm{CLVD}}| + |\Lambda_{\mathrm{DC}}| = 1, \tag{2a}$$

where

$$\Lambda_{\mathrm{ISO}} = \mathrm{sgn}\,(\zeta)\zeta^2, \tag{2b}$$

$$\Lambda_{\mathrm{DC}} = (1-\zeta^2)(1-\chi^2), \tag{2c}$$

$$\Lambda_{\mathrm{CLVD}} = \mathrm{sgn}\,(\chi)(1-\zeta^2)\chi^2. \tag{2d}$$

The above decomposition is suitable for source tensor determination by grid search as the number of parameters is not too large. The CAP inversion technique breaks each waveform into a Pnl window and a surface wave window (Zhao & Helmberger 1994; Zhu & Helmberger 1996). One advantage of doing so is that the two windows can be filtered in different frequency bands to optimize the degree of fit during the inversion. For each parameter combination, a set of synthetic waveforms is generated and windowed into the same Pnl and surface wave groups. In this study, the synthetics are formed using Green's functions computed with the method of Zhu & Rivera (2002) based on the 1-D southern California velocity model of Hadley & Kanamori (1977) (referred to below as HK77). The data and synthetic waveforms are cross-correlated and the synthetics are shifted to maximize the cross-correlation coefficients to help overcome inaccuracies in the assumed velocity model and event location.

In addition to the traditional parameters of strike, dip, rake, M_w and hypocentral depth, the gCAP inversions performed here also include ζ and χ to account for possible isotropic and CLVD source terms. The parameters are listed along with their respective grid-search ranges and step sizes in Table 1. The strike, dip, and rake are obtained by a brute-force grid search through the whole parameter space volume. The grid search for ζ, χ and M_w starts from zero initial values for ζ and χ and the catalogue magnitude for M_w, and continues with given step sizes until a minimum is found. The process is repeated at all possible source depths to find the best set of parameters, and is iterated at several step sizes to reduce the possibility of locking on local minima (Table 1). At the end of each grid search, a quadratic interpolation is performed in the neighbourhood of the grid point with minimum misfit to find the best parameter value and calculate the local curvature of the misfit surface for estimating the uncertainty of the value. As in Zhu & Helmberger (1996), the error function that is minimized is

Table 1. Ranges and step sizes for each of the parameters used in the inversions.

Parameter	Range	Step size
M_w	[1, 10]	0.1
Strike	[0, 360]	1
Dip	[0, 90]	1
Rake	[−180, 180]	1
ζ	[−1.0, 1.0]	0.05, 0.075, 0.1, 0.125, 0.15
χ	[−0.5, 0.5]	0.05, 0.075, 0.1, 0.125, 0.15
Depth	[3 km, 29 km]	2 km

given by,

$$e = \sum_{i=1}^{N} \left\{ \left[\left(\frac{r_i}{r_0} \right)^{p_{pnl}} w_{pnl} \left(u_{pnl} - s_{pnl} \right) \right]^2 + \left[\left(\frac{r_i}{r_0} \right)^{p_{sw}} \left(u_{sw} - s_{sw} \right) \right]^2 \right\}, \quad (3)$$

where N is the number of stations, r_i is the source–receiver distance, u and s denote the observed and synthetic seismograms, respectively, and parameters p_{pnl}, p_{sw}, w_{pnl} and r_0 have values of 1, 0.5, 2 and 100 km, respectively.

Minimal pre-processing is performed on the seismograms used for the inversions. The Pnl window length is 35-s-long and phases are filtered between 0.05 and 0.3 Hz, while the surface wave window is 70-s-long and phases are filtered from 0.02 to 0.1 Hz. The Green's functions are computed up to 10 Hz, and are used to identify *P*- and *S*-wave arrivals for windowing the seismograms into the Pnl and surface wave groups. Each component for every station is visually checked to confirm the quality of fit, and poorly fitting phases (e.g. those recorded on instruments located in basins) are often turned off. Additional inversion details including component weighting are documented in Zhu & Helmberger (1996).

We have chosen the region of study to be the geometrically complex trifurcation area of the San Jacinto fault zone (Fig. 1), where the primary fault structure splits into three subparallel strands. The trifurcation area also has one of the highest seismicity rates in California, and in particular produced 10 earthquakes with $M_w > 4$ in the last 15 yr. Nearly all of these earthquakes were recorded by over a hundred stations at local and regional scales, and the large amount of data helps to constrain the inversion results. The CAP method has been found to work best for stations up to approximately 300 km from the source, and this cut-off distance is used in our data analysis. The closest stations used are 40 km away from the epicentre to be consistent with the point-source and far-field approximations. The focal mechanisms shown in Fig. 1 are DC-constrained, derived by Yang *et al.* (2012) from first-motion polarities and amplitude ratios.

Using the gCAP procedure and parameters described above, we perform source tensor inversions for the seven $M_w > 4$ events shown in Fig. 1 without imposing deviatoric constraints. The results for the set of inversions are visually displayed in Fig. 2, with two focal mechanisms plotted for each earthquake. The unconstrained blue focal mechanisms include isotropic and CLVD components and can be compared to the yellow DC-constrained mechanisms obtained by the gCAP inversions. The red marks on each yellow focal mechanism show the station locations on the focal sphere used in the inversion for that event. An example map-view of the station configuration used for the 2013 March 13 M 4.7 is given by the blue triangles in Fig. 1. A sample of typical waveform fits is shown in Fig. 3 for a set of stations at two distance ranges. In general, the fitness is very good for each of the inversions performed.

Table 2 summarizes quantitative information on each event including retrieved isotropic and CLVD components, 95 per cent confidence limits (explained in Section 3), and results for statistical

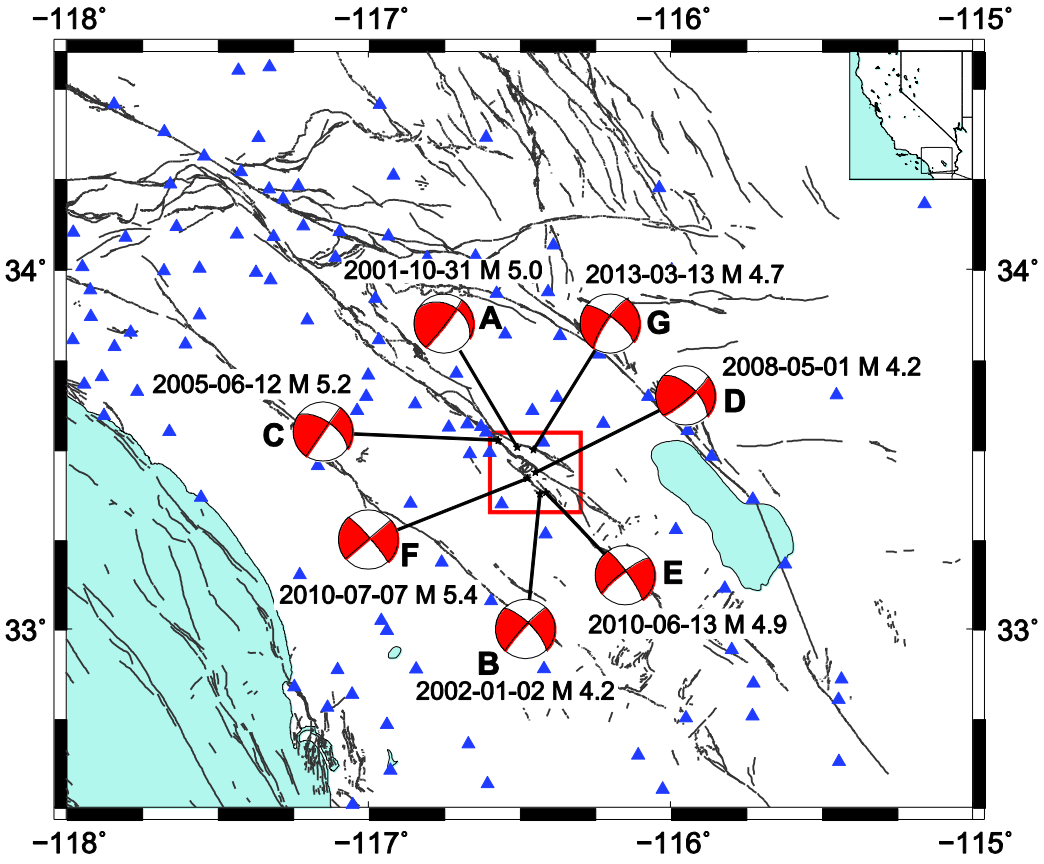

Figure 1. Map of the study area around the San Jacinto Fault Zone (SJFZ) in southern California (insert). Seven earthquakes with $M_w > 4.2$ in the complex trifurcation region (red box) of the SJFZ, denoted by a letter designation, are analysed (Table 2). The shown focal mechanisms are double-couple-constrained from the catalogue of Yang *et al.* (2012). The text near the mechanisms gives the date and magnitude of each event. The blue triangles denote the locations of stations used in the inversion of event G.

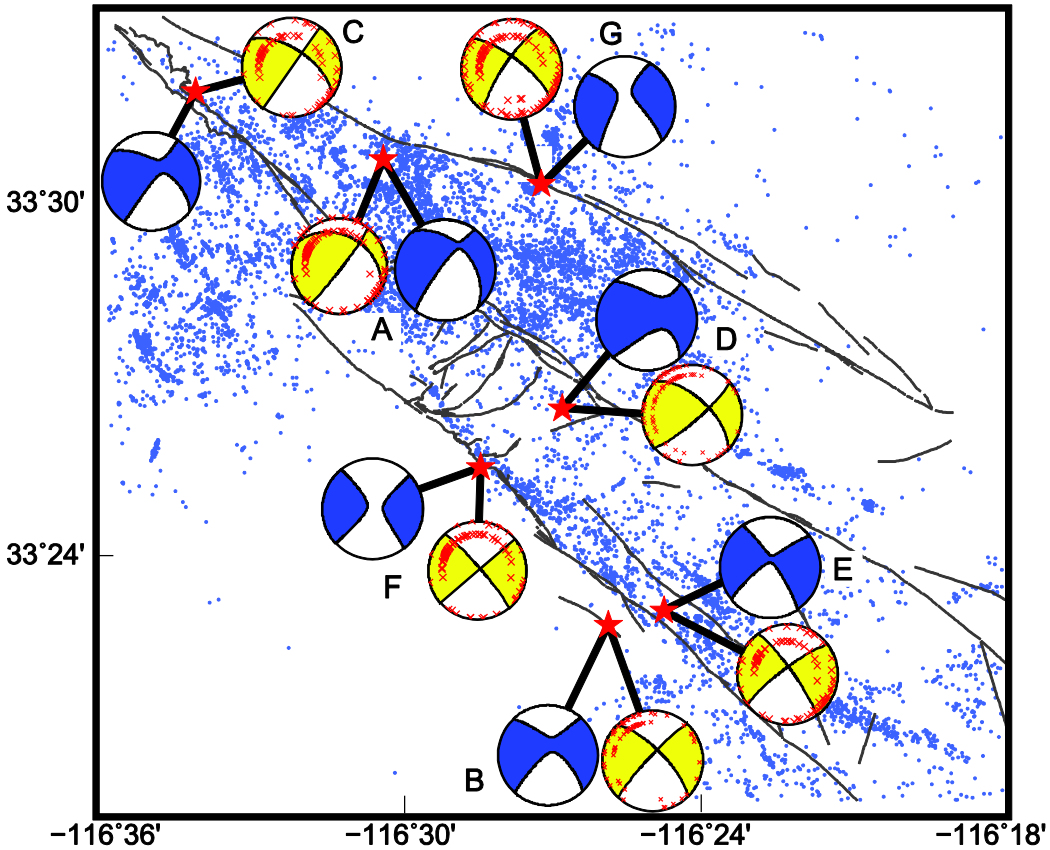

Figure 2. Inversion results for the analysed earthquakes. The blue focal mechanisms are unconstrained full source tensor solutions determined from gCAP waveform inversions. Each earthquake is found to have a small explosive isotropic component (see Table 2 for details). The yellow mechanisms are double-couple-constrained and shown with red '+' symbols that indicate the locations of stations used in the derivations. The blue dots are epicentres of background seismicity taken from the 1981 to 2011 catalogue of Hauksson *et al.* (2011).

significance. The isotropic components generally have small ζ values (eq. 1a) except for event D with ζ of 0.28. The corresponding per cent of the total potency (eqs 2a and 2b) taken up by the isotropic components ranges from 0.1 to 7.8 per cent. We note that all the isotropic terms are explosive in type as expected for brittle damage production during faulting (Ben-Zion & Ampuero 2009). The isotropic components remain explosive and similar in values when using a 1-D version of the double-difference velocity model of Allam & Ben-Zion (2012) for the plate-boundary region around the SJFZ. The estimated CLVD components are also small, but frequently reverse sign. The parameter values for the HK77 velocity model are summarized in Table 3. We demonstrate in the subsequent section that these CLVD components are generally not statistically significant.

While a significant number of stations have been used in each inversion, this alone does not give confidence for the small derived isotropic components. In the next section we describe a number of statistical techniques used to quantify the uncertainty involved in the inverse problem, and show how the uncertainties are compared to the values summarized in Table 2.

3 TESTS FOR STATISTICAL ROBUSTNESS

3.1 Bootstrap analysis

It is well known that using classical statistics to estimate the uncertainty for a single inversion is quite limited. However, the bootstrap theorem (Efron 1979) allows one to resample the stations used in an inversion to quantify the variability present. We applied the bootstrap theorem to each of the events investigated in this study by randomly choosing stations with replacement from the set of stations used in the inversion. The number of stations resampled is equal to the number used for the results described in Fig. 2; this leads to some being repeated multiple times while others are omitted. For example, the inversion of event G involved 126 stations, so for each bootstrap iteration 126 stations were randomly chosen from this original set of 126, with replacement, to create a resampled station configuration. A new inversion is performed using the resampled data set to obtain a new estimate for each of the inversion parameters. This process is repeated 1000 times, giving a statistical description of the variability possible. The inversion values for the strike, dip, rake, depth and moment are well resolved and consistent with results reported by the DC-constrained focal mechanism catalogues of Yang *et al.* (2012). Further, the strike, dip, rake and M_w are almost identical for different values of ζ and χ. In contrast, the isotropic and CLVD components are small and variable, and thus are the focus of the bootstrap analysis.

Fig. 4 presents a histogram of isotropic components resulting from the bootstrap procedure for each of the events (Fig. 4a), along with an empirical cumulative distribution function (ECDF) for each event (Figs 4a and b). The bootstrap histograms give a sense for how frequently the inversions are converging to a particular value when the station configuration is varied. If the standard deviation of the histogram is small, it suggests uniformity among the results for all stations and adds greater confidence to the best-fitting parameter

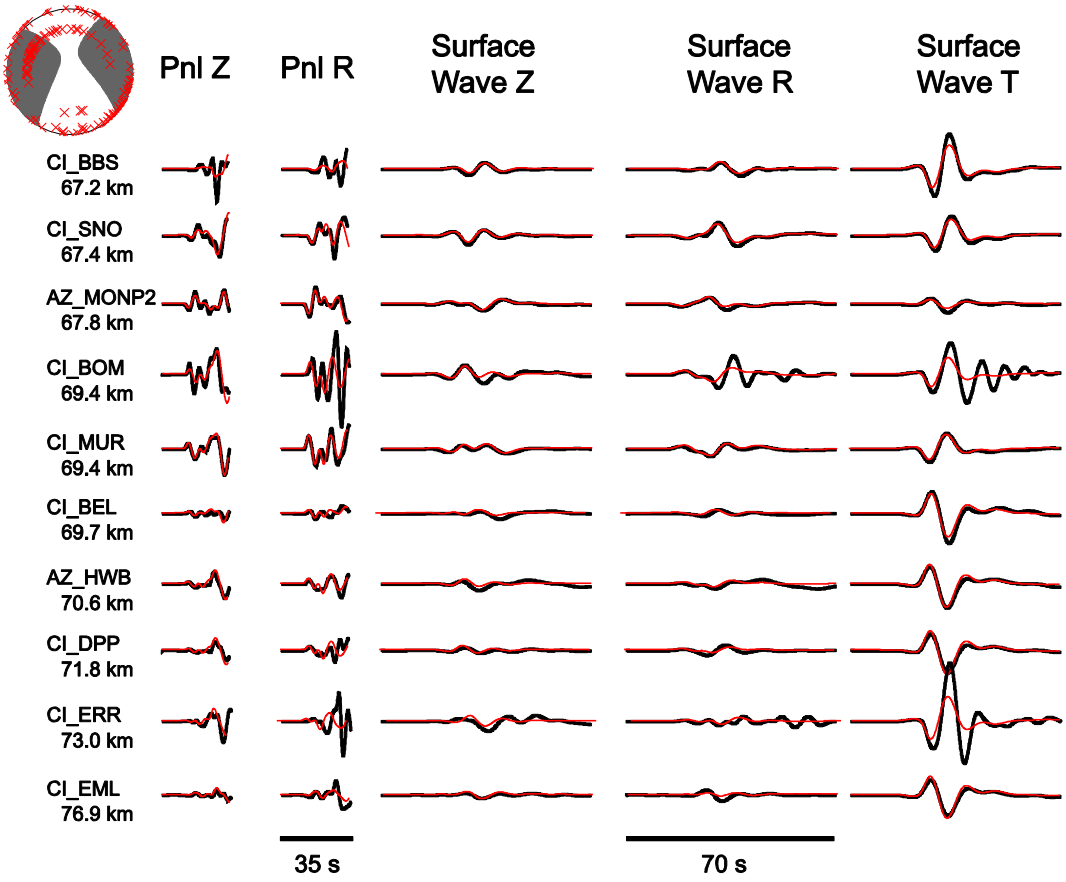

Figure 3. Sample of data (black) and calculated (red) waveforms for 10 stations used for the 2013 March 13 earthquake (Event G). Phase components from left to right are vertical Pnl, radial Pnl, vertical surface waves, radial surface waves and tangential surface waves. The shown focal mechanism is unconstrained with station locations used in the derivations marked by red '+' symbols. The positive directions of motion for the different windows are: vertical (up), radial (outward) and transverse (clockwise).

Table 2. Results of the source tensor gCAP inversions for the analysed earthquakes (Fig. 2). Confidence intervals for ζ (eqs 1a and b) are derived from bootstrapping. The entries ζ ($\chi = 0$) correspond to best-fitting isotropic terms when the CLVD is constrained to be zero. All other inversion parameters are derived from full (unconstrained) tensor inversions. VR denotes variance reduction and NS denotes number of stations used for each inversion.

Event	Date	Time	Lat.	Lon.	Depth (km)	M_w	Strike	Dip	Rake	ζ	ζ: 95 per cent CI	χ	ζ ($\chi = 0$)	% ISO	VR	NS
A	10/31/2001	07:56:16.630	33.51	−116.51	17	5	218	82	−47	0.10	[0.05, 0.14]	0.00	0.10	1.0	70	104
B	1/2/2002	12:11:28.680	33.37	−116.43	15	4.2	223	85	−18	0.11	[0.4, 0.24]	0.04	0.11	1.2	76	71
C	6/12/2005	15:41:46.540	33.53	−116.57	13	5.2	216	90	−28	0.06	[−0.01, 0.16]	0.01	0.08	0.4	80	102
D	5/1/2008	03:55:35.970	33.44	−116.45	11	4.2	49	77	29	0.28	[0.18, 0.35]	−0.03	0.28	7.8	64	85
E	6/13/2010	03:08:57.090	33.38	−116.42	11	4.9	234	77	−9	0.06	[0.0, 0.10]	−0.04	0.04	0.4	75	85
F	7/7/2010	23:57:23.040	33.42	−116.48	13	5.4	49	90	5	0.03	[−0.02, 0.08]	−0.09	0.00	0.1	73	96
G	3/13/2013	16:56:06.040	33.50	−116.46	13	4.7	216	81	−16	0.16	[0.07, 0.20]	−0.04	0.14	2.6	78	126

Table 3. Parameters of the HK77 velocity model.

Layer depth (km)	V_P (km)	V_S (km)	Q_P	Q_S
5.5	5.5	3.18	1200	600
16.0	6.3	3.64	1200	600
32.0	6.7	3.87	1200	600
9999	7.8	4.50	1800	900

value. The ECDF gives the percentage of times that a resampled inversion produces an isotropic or CLVD component in a given range, which allows calculating confidence limits for the parameters. The vertical axis of the ECDF indicates percentile (in probability units) and the horizontal axis indicates the values of a given parameter (ζ or χ). Confidence intervals and hypothesis tests can be computed by reading off the value of the horizontal axis of the ECDF that corresponds to a specific percentile.

We first perform a statistical hypothesis test that the isotropic component is explosive in type. Formally stated, we test a null hypothesis that the isotropic component is less than or equal to zero, and an alternative hypothesis that the isotropic component is greater than zero (explosive). This is based on the expectation from laboratory results and theory that brittle deformation (in the earthquake source volume) is associated with rock dilation (Ben-Zion & Ampuero 2009; Hamiel *et al.* 2009; Lockner *et al.* 1977). If a 95 per cent confidence level is desired for a 1-tailed hypothesis test, we use the ECDF to determine whether 95 per cent of the resampled inversions produced an isotropic component greater

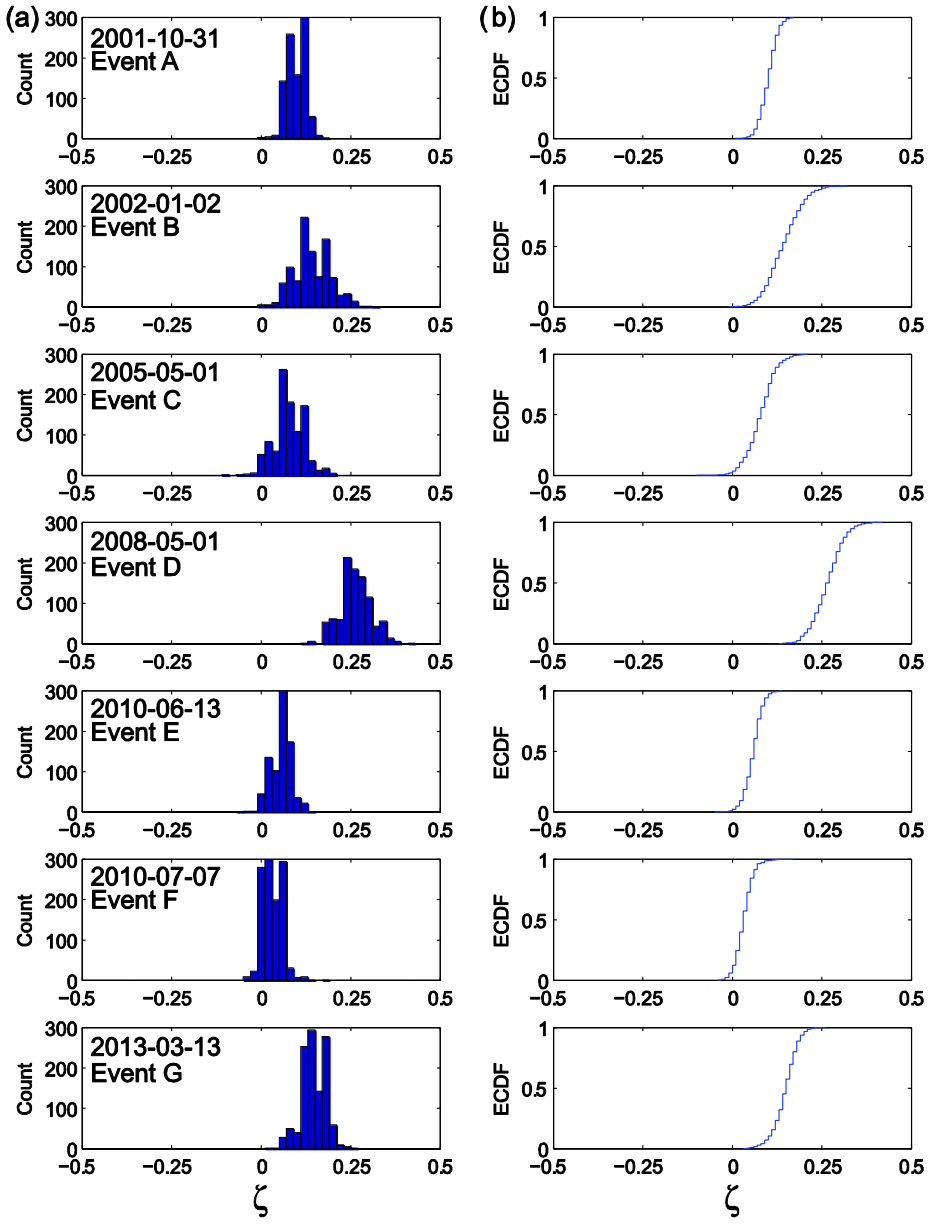

Figure 4. (a) Bootstrap distributions of the isotropic components of each event (different panels) obtained from resampling stations with replacement from the set used to perform the inversions shown in Fig. 2. For each event 1000 inversions are performed with a resampled station configuration. (b) Empirical cumulative distribution functions (ECDF) corresponding to each bootstrap distribution in (a). Each ECDF is used to obtain confidence limits and perform hypothesis tests for an explosive isotropic component. Six out of the seven earthquakes are found to have statistically significant values at the 95 per cent confidence level, with the last one being significant at the 90 per cent confidence level.

than zero. If this is true, then the isotropic component is statistically significant with regards to the bootstrap procedure at the 95 per cent confidence level and the null hypothesis is rejected. Such a procedure is non-parametric and avoids the stringent requirement that the data are drawn from a normally distributed population.

Examination of the ECDF for the 7 analysed events suggests that the isotropic components are statistically significant at the 95 per cent confidence level, except for event F (Figs 1 and 2) that has a statistically significant isotropic term at a 90 per cent confidence level. One primary reason we can demonstrate significance for these events is that the amount of data used for each inversion is unusually large for regional inversions. We note, however, that it is the explosive nature of the isotropic components that is found to be robust rather than the best-fitting numerical values. Further, while statistical significance via the bootstrap theorem is encouraging, these tests implicitly assume that the Green's functions are correct. Perturbations to the Green's functions are addressed in Section 3.4.

Fig. 5 shows corresponding results associated with applying bootstrap resampling to the CLVD components for each event. In contrast to the calculations for the isotropic components, the ECDF panels (Fig. 5b) indicate that five of the seven events do not have statistically significant CLVD components at the 95 per cent confidence level. It is clear from the histograms (Fig. 5a) that the sign of the CLVD component regularly flips depending on the stations used, which is in direct contrast to the isotropic component. The bootstrap resampling calculations indicates that the non-zero CLVD for these earthquakes may be an artefact of the inversion process.

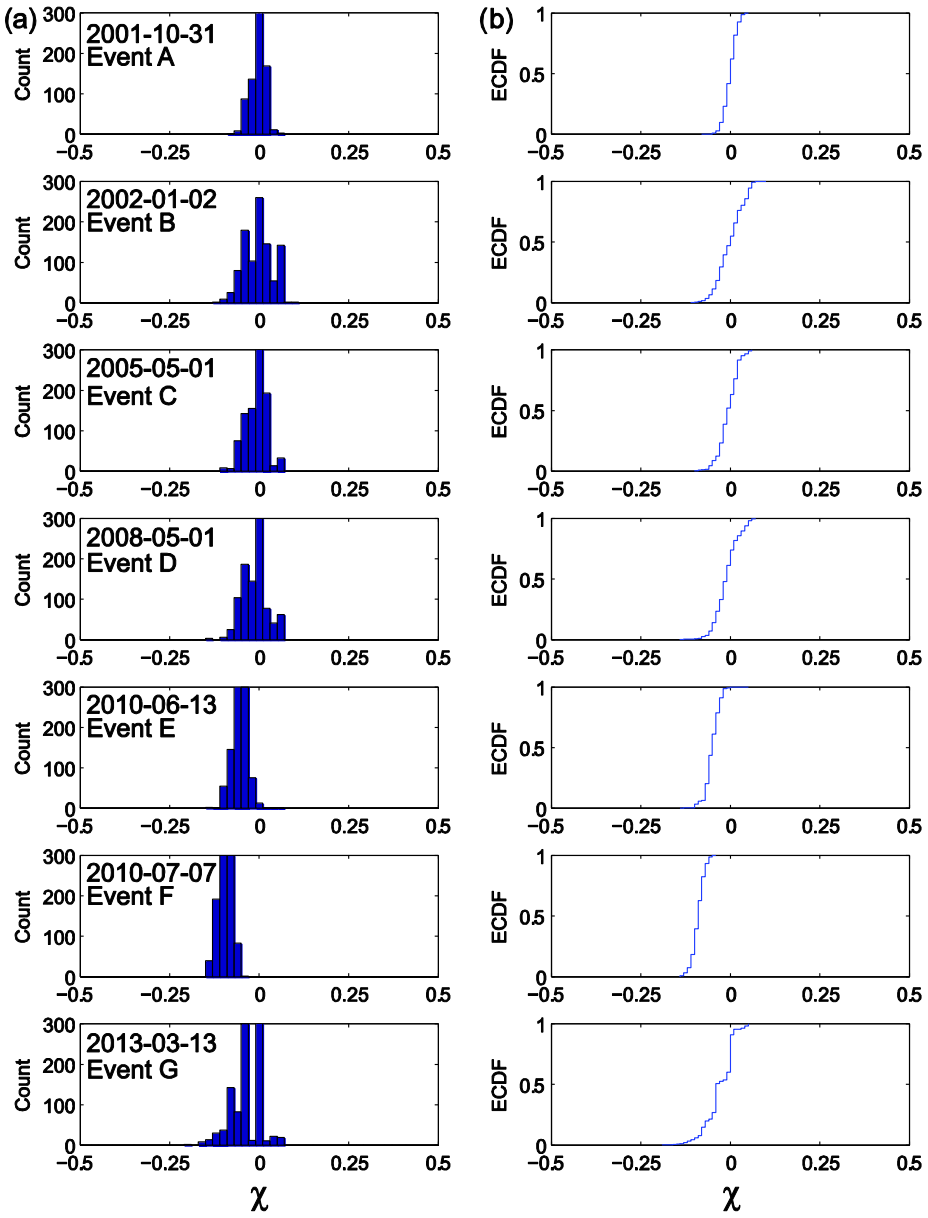

Figure 5. Same as Fig. 4, but for CLVD components. Five of the seven events have CVLD components that are not statistically significant, which indicates they are likely artefacts of the inversion process.

3.2 ISO to CLVD partitioning

A number of studies (Kawakatsu 1991, 1996; Hara *et al.* 1995, 1996) examined the possibility of isotropic components in deep earthquakes primarily as evidence for polymorphic phase transitions. These studies have paid careful attention to parameter trade-off in the inversion process, most notably between an isotropic component and vertically oriented CLVD sources. This trade-off can occur when there is limited focal sphere coverage that is constrained primarily to the sphere's edges. This is because the radiation pattern for a vertically oriented CLVD is reminiscent of an explosion pattern in these areas, and in particular is constant in an azimuthal direction. However, the results from these studies of deep earthquakes at teleseismic distances may not necessarily translate at a regional scale with shallow crustal earthquakes.

To examine the trade-off present in the gCAP inversion process for the San Jacinto fault zone earthquakes, the inversions are first repeated while constraining the CLVD component to be zero. This allows us to understand how much the isotropic component for these specific results is influenced by the CLVD component. As indicated in Table 2, the isotropic components generally do not change in any significant way by the constraints $\chi = 0$, and each remains explosive in type (except for event F, which is less statistically significant).

To more rigorously study whether the isotropic component can map into the CLVD term, we conduct a series of synthetic inversions using a realistic station configuration. We assume the exact configuration used for the inversion of the 2013 M_w 4.7 event G, and generate synthetic waveforms with pure deviatoric (DC + CLVD) sources. Three different types of DC orientations are used corresponding to the basic source types of strike-slip, reverse and normal with 45° dips. For each, we generate synthetics with different values of χ and then perform an inversion while constraining the source to have only DC and isotropic terms. The range of χ values is from -0.5 to 0.5 in increments of 0.01. Non-zero values of ζ retrieved

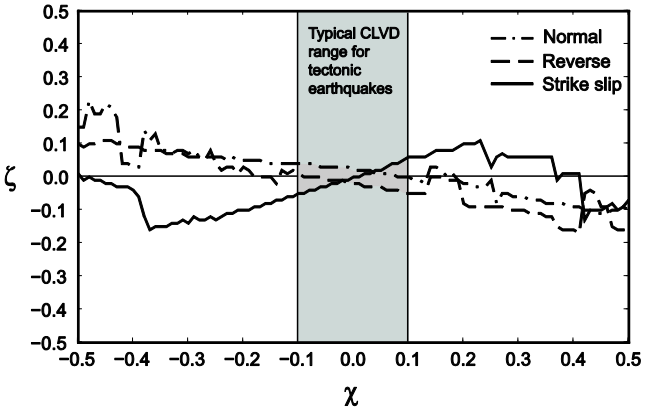

Figure 6. Summary of synthetic tests for isotropic-CLVD trade-off. Synthetic deviatoric waveforms are created for the station configuration used for event G (Fig. 2) for a given CLVD strength (horizontal axis). The synthetic waveforms are inverted with the constraint of zero CLVD term. The obtained isotropic values shown on the vertical axis describe parameter mapping and isotropic component error. For the range of CLVD values typical of tectonic earthquakes, the artificially retrieved isotropic components are generally smaller than isotropic components obtained in this study (Table 2).

by these inversions are artefacts of CLVD components mapping into ζ.

Fig. 6 summarizes the results of the synthetic tests, with retrieved ζ values on the vertical axis and used χ values on the horizontal. For CLVD components smaller than 0.15, which is a generous upper limit on our derived χ values (Table 2), the isotropic components retrieved are no larger than 0.08. The retrieved ζ values corresponding to $\chi = 0.1$ are around 0.05, which is smaller than all of the statistically significant isotropic components found for the SJFZ earthquakes (Table 2). Furthermore, this test assumes that all of the CLVD is mapping into the DC and isotropic components, whereas we allow χ to be a free parameter in our data inversions. These findings are in agreement with the fact that the isotropic components in the SJFZ earthquakes remain largely unchanged when constraining the CLVD component to be zero. From the CVLD bootstrap tests (Fig. 5), it is clear that the CLVD term regularly takes on both positive and negative values for all of the events. For strike-slip focal mechanisms, however, only a positive CLVD component can map into an explosive isotropic component. This provides additional evidence that CLVD components are unlikely to be responsible for derived isotropic components that are all explosive. Given the lack of significant trade-off between the CLVD and ISO components in our case, and the fact that the CLVD terms of the analysed events are not statistically significant (Fig. 5), we perform additional studies of significance in the next subsections only on the isotropic components.

3.3 *F*-test analysis

One popular method of assessing the statistical significance of including an additional parameter in a regression model is the *F*-test. Using the *F*-test in source tensor inversions for isotropic components may be helpful (e.g. Dreger *et al.* 2000), but should not be thought of in the same way as a traditional regression model for several reasons. First, seismic data are known to not have normally distributed errors, which is a requirement of the *F*-test for true statistical significance. Second, the isotropic component has a very weak effect on the variance reduction. For example, if a true source has an isotropic component of $\zeta = 0.3$, inverting the waveforms while constraining $\zeta = 0$ will only lower the variance reduction by a couple per cent as compared with an unconstrained inversion. The *F*-test is directly based on large changes in the variance reduction, so it a poor choice from a theoretical standpoint for testing small isotropic components, regardless of how accurate the Green's functions are. We conducted synthetic inversions with varying degrees of ζ, and found that even synthetic waveforms are not statistically significant with the *F*-test for $\zeta < 0.4$. As a result, it is not informative to use the *F*-test for events with $\zeta < 0.1$ as those analysed in this study.

3.4 Velocity model perturbations

It is possible that the derived isotropic components result from inaccuracies in the velocity model that propagate through the inversion. This has been shown to be a valid explanation for some CLVD components (Kuge & Lay 1994), in addition to their artificial generation by non-planar fault geometries, in derivations using the point source approximation (e.g. Julian *et al.* 1998). To examine whether reasonable velocity perturbations can produce uncertainties larger than the derived isotropic components, we perform two types of tests.

The first test involves generating 500 different velocity models that are randomly perturbed from the original HK77 model. The perturbations are done to the thickness, depth, shear wave velocity, and the ratio of *P* over shear velocity of each layer. The perturbations to each parameter are drawn from a uniform distribution between [−5 per cent, 5 per cent] of the original value for that quantity. The value of 5 per cent is generally the upper bound on uncertainty in the HK77 model over the analysed frequency range compared with a number of recent 3-D tomography studies in the study region (Allam & Ben-Zion 2012; Allam *et al.* 2014; Zigone *et al.* 2015). For each event, we generate Green's functions for each of the perturbed 500 velocity models and create 500 sets of synthetic DC seismograms. The DC orientation is taken from the focal mechanism catalogue of Yang *et al.* (2012), and we invert each set of synthetics using the non-perturbed HK77 model. The synthetic seismograms are created for the exact station configuration of each earthquake as used previously (Fig. 2). If the events are really due to pure DC sources, and the true velocity model corresponds to one of the perturbed cases, the error introduced by using the non-perturbed HK77 model can be quantified. This is done by comparing the isotropic components obtained from these synthetic tests with a test distribution, such as the bootstrap results, in the form of a hypothesis test to see whether they are distinctly different.

The resulting distribution of ζ values (blue) is plotted in Fig. 7 alongside the previously obtained bootstrap histogram (red) of each event. We use a Mann–Whitney *U* test (Hollander & Wolfe 1973) to examine whether the values in one sample are statistically larger than the other. The tests indicate that for each event, the bootstrap distribution is statistically larger than the velocity perturbation distribution at the 99 per cent confidence level. This suggests that the values obtained from the data inversions (Table 2) are unlikely to be the result of velocity model errors. These results are visually seen by the clear separation (and relatively little overlap) between the red and blue histograms for each event in Fig. 7. It is notable that the velocity model perturbations create both positive and negative isotropic components from the errors. If we approximate the distribution as being 50 per cent explosive with the sign chosen at random for an artificial isotropic component produced by velocity model errors, the probability of all events having an explosive type as the result of velocity model errors is 0.5^7 which is 7.81E-03.

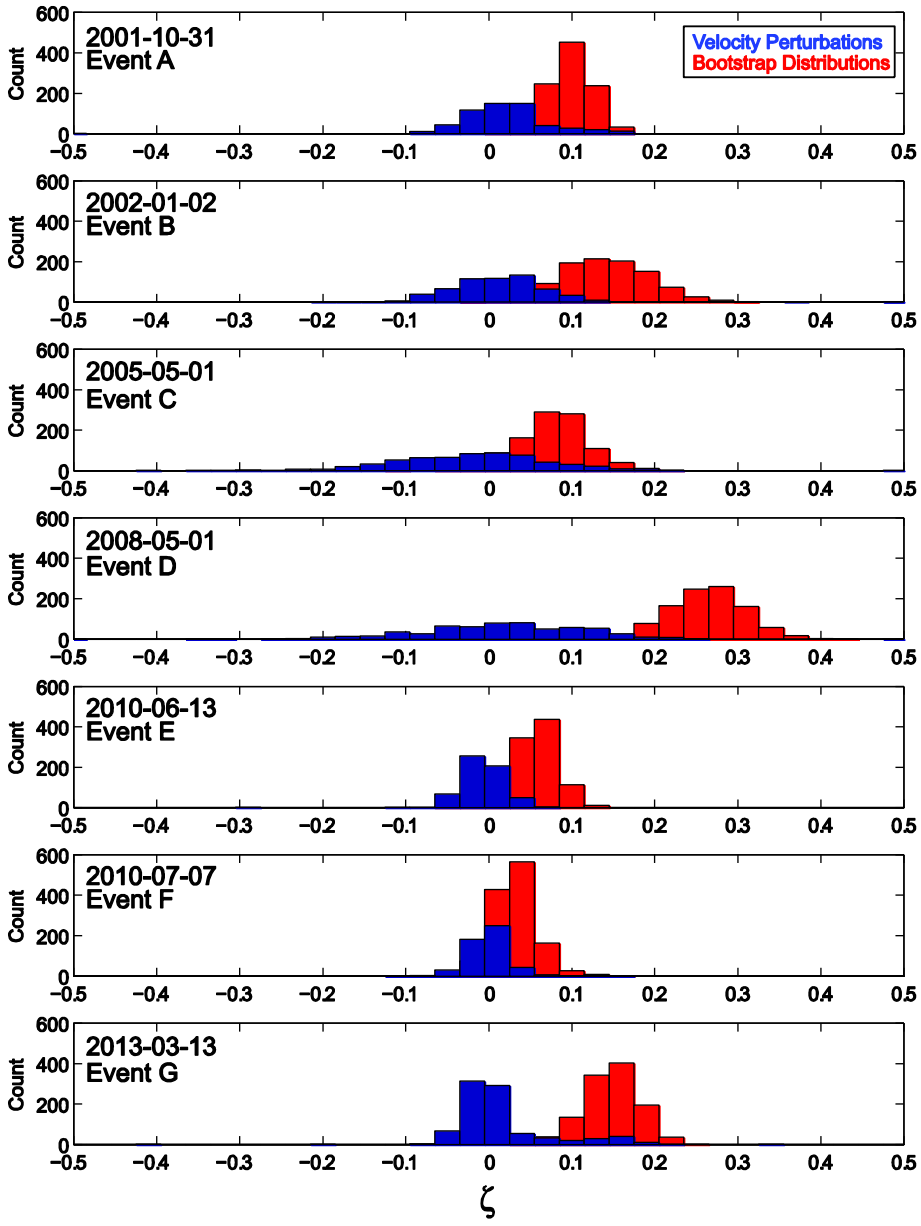

Figure 7. Results of the first type of velocity model perturbation tests. The DC-constrained focal mechanism of each earthquake (Fig. 1) is used to create synthetic DC waveforms from 500 different perturbed velocity models at the same station configuration as the original inversion (Fig. 2). Each set of synthetics for a perturbed model is inverted using the HK77 velocity model while allowing isotropic and CLVD components. The obtained values of isotropic terms (blue histogram) are plotted alongside the values obtained from the bootstrap distribution (red) of Fig. 4. Comparisons via the Mann–Whitney *U*-test indicate that all 7 of the examined earthquakes have bootstrap distributions that are statistically larger than the distributions obtained from the perturbed velocity models at the 99 per cent confidence level.

An alternative method of testing the sensitivity of the isotropic component to velocity model errors involves performing a new inversion on the observed waveforms with each perturbed model. This is the opposite of the previous test, which inverted synthetic waveforms calculated for DC sources and the perturbed models. The resulting isotropic components in this second test can also represent the uncertainty limits due to errors in the velocity model on the values indicated in Table 2. Fig. 8 shows the obtained histograms for each event (Fig. 8a) and the corresponding ECDF (Fig. 8b). Four of the seven events have isotropic components that are explosive ($\zeta > 0$) for more than 95 per cent of the perturbed models, while the remaining three have isotropic components that are explosive over 70 per cent of the cases. In two events (D and G) the isotropic components are explosive over 99 per cent of the time, so clearly several of these earthquakes have statistically significant explosive isotropic components with respect to the velocity model perturbations.

We also performed both of the model perturbation tests using a different randomly drawn model at each station. For both test scenarios the statistical conclusions remain the same as discussed above. The conducted velocity model tests lead us jointly to conclude that the basic aspects of the derived results on isotropic source terms are unlikely due to errors in the HK77 model.

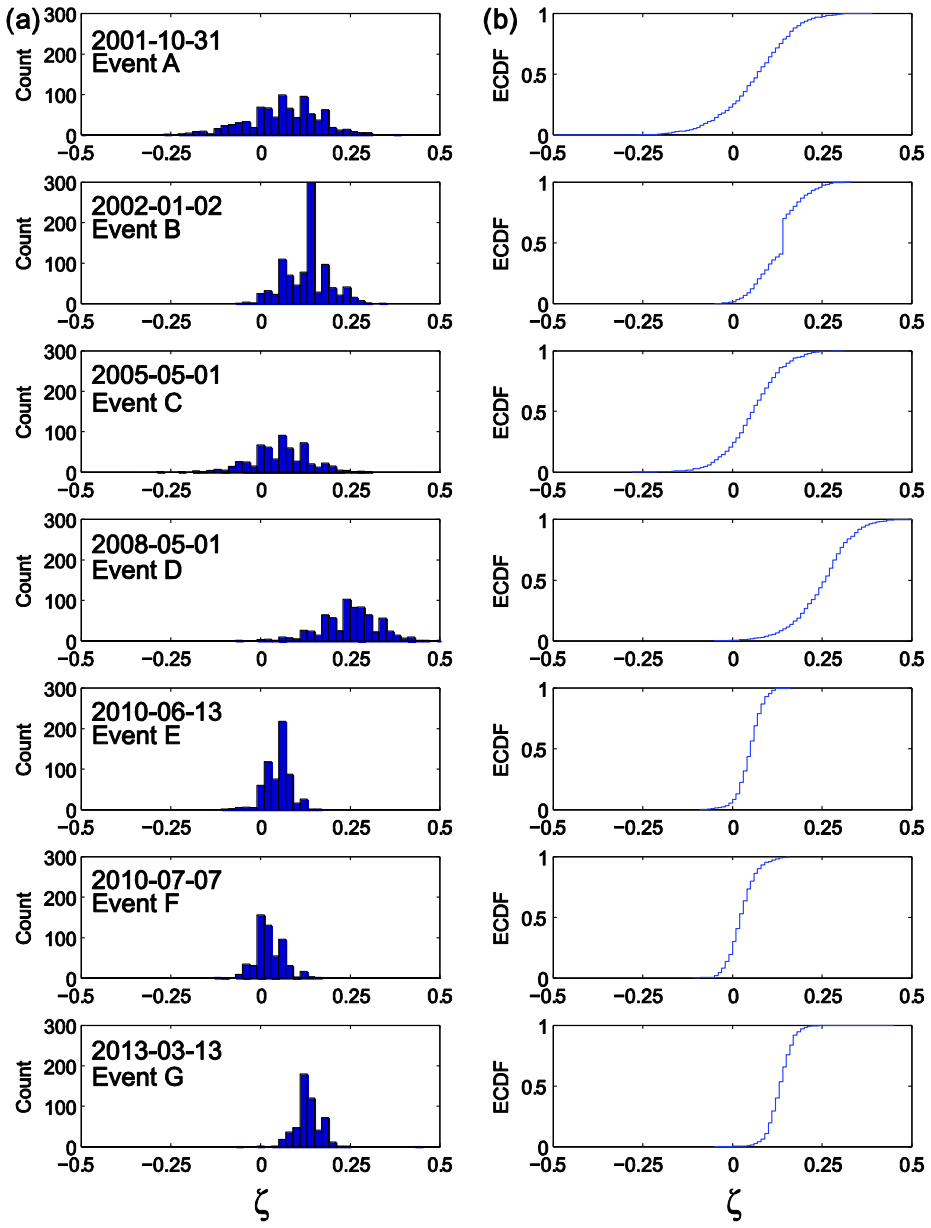

Figure 8. Results of the second type of velocity model perturbation tests. Each earthquake is inverted 500 times using Green's functions from a randomly perturbed velocity model to quantify the uncertainty in the isotropic component due to model choice. (a) Histograms of isotropic components for each event (different panels). (b) Empirical cumulative distribution functions corresponding to each sample in (a). The ECDF are used to perform hypothesis testing for explosive isotropic components. Four of the seven events have statistically significant isotropic components at the 95 per cent level, one at the 90 per cent level and two at about the 70 per cent level.

4 DISCUSSION

Resolving isotropic source terms of regular tectonic earthquakes is very challenging since the events are dominated by shear deformation. Trade-offs between parameters of the CLVD and isotropic components and uncertainties in the used velocity model can produce additional difficulties. For these reasons routine inversions of seismic waveforms for source mechanisms constrain the inversions to be purely deviatoric (and often purely DC). While this is appropriate for studies interested in the overall kinematics of the source, brittle fracturing is expected to be associated generally with an isotropic source term (Ben-Zion & Ampuero 2009). The existence of small isotropic radiation in earthquake rupture zones can change dramatically the physics of the local failure process, with significant implications for many topics ranging from the heat flow paradox to the crack vs. slip mode of earthquake rupture (Brune *et al.* 1993; Ben-Zion 2001, and references therein). Clarifying the extent of isotropic earthquake source terms is also important for discrimination of small explosions from earthquakes, which rely largely on *P*/*S* ratios of recorded seismograms (e.g. Walter *et al.* 1995).

A number of recent studies found evidence in support of isotropic components of regular tectonic earthquakes in areas likely associated with brittle fracturing. Ross & Ben-Zion (2013) examined DC constrained focal mechanism catalogues of the 1992 Landers, CA earthquake sequence. They found systematic spatio-temporal variations in rotations of aftershock focal mechanisms with strong variations near the edges of the rupture zone (especially around

the NW end). They showed with synthetic calculations that the observed spatial heterogeneity of rotations can result from neglecting isotropic components with $\zeta = 0.03$–0.15 when constraining the focal mechanisms to be DCs. This estimated range of ζ is in agreement with the values obtained in this study (Table 2). Castro & Ben-Zion (2013) analysed spectral ratios of seismograms generated by pairs of colocated aftershocks of the 2010 M_w 7.2 El Mayor-Cucapah earthquake. They observed amplification of $\underline{P}$ radiation of about 5–10 in the frequency range 1–10 Hz that is consistent with isotropic source components produced by rock damage. Kwiatek & Ben-Zion (2013) derived ratios of *S*-to-*P* radiated energy (E_S/E_P) of >500 well-recorded small earthquakes in the Mponeng deep gold mine, South Africa. Many E_S/E_P ratios were relatively low (median value <5), suggesting tensile source components and enhanced *P* radiation for many events consistent with rock damage in the source volumes. The examined frequency ranges by Castro & Ben-Zion (2013) and Kwiatek & Ben-Zion (2013) are well beyond the 0.3 Hz maximum used in this work, and may be where the brittle damage is manifest more strongly. This is because the networks of microfractures created during the damage process may be significantly smaller than the overall size scales of the shearing sources.

Our results indicate small explosive isotropic source terms of crustal earthquakes in a complex region of the San Jacinto fault zone in southern California. The analysis is based on waveform inversions of data recorded by many three-component stations at distances no more than 300 km from the sources. Previous studies calling attention to parameter correlation between isotropic and CLVD sources (Kawakatsu 1991, 1996; Hara *et al.* 1995, 1996) primarily focused on earthquakes with focal depths of hundreds of kilometres, using recordings obtained at teleseismic distances. These studies typically used centroid moment tensor inversions with a greater number of parameters than used in this work, and considered data in a considerably lower frequency range (20–1000 s) than the ones used in our work (3–20 s for body waves and 10–50 s for surface waves). Also, in several of the aforementioned studies the retrieved isotropic components regularly flip sign between implosive and explosive sources, which is typical for inversion artefacts, in contrast to our results where all isotropic components are found to be explosive (Table 2).

Dufumier & Rivera (1997) extensively analysed the capability of extracting information related to the isotropic component from seismograms in terms of resolution and correlation matrices, with emphasis on inversions at teleseismic distance scales in different frequency bands than the ones used here. They discussed the instability of the isotropic component under certain conditions, but such instabilities are not observed in this work. Also, the joint inversion performed here weights the Pnl and surface wave groups differently to keep the larger amplitude arrivals from dominating the inversion (Zhu & Helmberger 1996), an issue raised by Pearce & Rogers (1989) and Dufumier & Rivera (1997).

The earthquakes analysed in this work, as well as in the studies of Ross & Ben-Zion (2013), Castro & Ben-Zion (2013) and Kwiatek & Ben-Zion (2013), did not occur on geometrically simple faults that may fail by frictional sliding alone. Some rock fracturing, and hence damage-related-radiation, is expected to accompany the earthquake source process in such locations. However, we cannot rule out that additional mechanisms such as seismic anisotropy, faulting on non-planar surfaces and fluid effects contribute to the observed isotropic radiation (e.g. Julian *et al.* 1998). Some of these mechanisms are likely to co-exist; for example, faulting on non-planar faults and near rupture ends should lead to rock damage (e.g. Ben-Zion 2008, section 6) and brittle rock damage can produce seismic anisotropy in the source region (e.g. Hamiel *et al.* 2009). The damage-related-radiation is expected to be relatively large in area without well-defined pre-existing faults and relatively small on geometrically simple fault sections. We also expect shallower events to produce more damage-related-radiation than deeper ones. These expectations should be tested in future studies involving larger areas and larger number of events.

To check whether the isotropic source terms derived for the seven analysed events (Figs 1 and 2) could be considered robust, we conducted bootstrap analysis, examined isotropic to CLVD partitioning, and explored the effects of velocity model perturbations on the retrieved isotropic components. Collectively, these tests suggest that the isotropic components derived for most or all of the events are statistically robust. Each of the examined earthquakes is found to have a small explosive isotropic component that may reflect damage-related-radiation stemming from brittle cracking in the source volumes. To increase the confidence that regular tectonic earthquakes (in geometrically complex regions) have isotropic source terms that may reflect damage-related-radiation, it would be useful to incorporate in the analysis 3-D Green's functions, include higher frequencies in the inversion process and examine data of additional events. Work on these topics will be done in future studies.

ACKNOWLEDGEMENTS

The study was supported by the National Science Foundation (grants EAR-0838195 and EAR-1249701). The paper benefitted from useful comments of an anonymous referee and Editor Eiichi Fukuyama.

REFERENCES

Aki, K. & Richards, P.G., 2002. *Quantitative Seismology,* 2nd edn, University Science Books, Sausalito, CA, USA.

Allam, A.A. & Ben-Zion, Y., 2012. Seismic velocity structures in the Southern California plate-boundary environment from double-difference tomography, *Geophys. J. Int.,* **190,** 1181–1196.

Allam, A.A., Ben-Zion, Y., Kurzon, I. & Vernon, F.L., 2014. Seismic velocity structure in the Hot Springs and Trifurcation Areas of the San Jacinto Fault Zone, California, from double-difference tomography, *Geophys. J. Int.,* **198,** 978–999.

Ampuero, J.-P. & Dahlen, F.A., 2005. Ambiguity of the moment tensor, *Bull. seism. Soc. Am.,* **95,** 390–400.

Backus, G. & Mulcahy, M., 1976a. Moment tensors and other phenomenological descriptions of seismic sources—I. Continuous displacements, *Geophys. J. R. astr. Soc.,* **46**(2), 341–361.

Backus, G. & Mulcahy, M., 1976b. Moment tensors and other phenomenological descriptions of seismic sources—II. Discontinuous displacements, *Geophys. J. R. astr. Soc.,* **47**(2), 301–329.

Ben-Zion, Y., 2001. Dynamic ruptures in recent models of earthquake faults, *J. Mech. Phys. Solids,* **49**(9), 2209–2244.

Ben-Zion, Y., 2003. Appendix 2, Key Formulas in Earthquake Seismology, in *International Handbook of Earthquake and Engineering Seismology,* eds Lee, W.H.K., Kanamori, H., Jennings, P.C. & Kisslinger, C., Part B, pp. 1857–1875, Academic Press.

Ben-Zion, Y., 2008. Collective behavior of earthquakes and faults: continuum-discrete transitions, progressive evolutionary changes and different dynamic regimes, *Rev. Geophys.,* **46,** RG4006, doi:10.1029/2008RG000260.

Ben-Zion, Y. & Ampuero, J., 2009. Seismic radiation from regions sustaining material damage, *Geophys. J. Int.,* **178**(3), 1351–1356.

Brune, J., Brown, S. & Johnson, P., 1993. Rupture mechanism and interface separation in foam rubber models of earthquakes: a possible solution to the

heat flow paradox and the paradox of large overthrusts, *Tectonophysics,* **218,** 59–67.

Castro, R.R. & Ben-Zion, Y., 2013. Potential signatures of damage-related radiation from aftershocks of the 4 April 2010 (Mw 7.2) El Mayor-Cucapah Earthquake, Baja California, México, *Bull. seism, Soc. Am.,* **103,** 1130–1140.

Chapman, C. & Leaney, W., 2012. A new moment-tensor decomposition for seismic events in anisotropic media, *Geophys. J. Int.,* **188**(1), 343–370.

Dor, O., Yildirim, C., Rockwell, T.K., Ben-Zion, Y., Emre, O., Sisk, M. & Duman, T.Y., 2008. Geologic and geomorphologic asymmetry across the rupture zones of the 1943 and 1944 earthquakes on the North Anatolian Fault: possible signals for preferred earthquake propagation direction, *Geophys. J. Int.,* **173,** 483–504.

Dreger, D.S., Tkalcic, H. & Johnston, M., 2000. Dilatational processes accompanying earthquakes in the Long Valley Caldera, *Science,* **288,** 122–125.

Dufumier, H. & Rivera, L., 1997. On the resolution of the isotropic component in moment tensor inversion, *Geophys. J. Int.,* **131**(3), 595–606.

Efron, B., 1979. Bootstrap methods: another look at the jackknife, *Ann. Statist.,* **7,** 1–26.

Hadley, D. & Kanamori, H., 1977. Seismic structure of the Transverse Ranges, California, *Geol. Soc. Am. Bull.,* **88**(10), 1469–1478.

Hardebeck, J. & Shearer, P., 2002. A new method for determining first-motion focal mechanisms, *Bull. seism. Soc. Am.,* **92**(6), 2264–2276.

Hamiel, Y, Lyakhovsky, V., Stanchits, S., Dresen, G. & Ben-Zion, Y., 2009. Brittle deformation and damage-induced seismic wave anisotropy in rocks, *Geophys. J. Int.,* **178,** 901–909.

Hara, T., Kuge, K. & Kawakatsu, H., 1995. Determination of the isotropic component of the 1994 Bolivia deep earthquake, *Geophys. Res. Lett.,* **22**(16), 2265–2268.

Hara, T., Kuge, K. & Kawakatsu, H., 1996. Determination of the isotropic component of deep focus earthquakes by inversion of normal-mode data, *Geophys. J. Int.,* **127**(2), 515–528.

Hauksson, E., Yang, W. & Shearer, P.M., 2011. Waveform relocated earthquake catalog for Southern California (1981 to June 2011), *Bull. seism. Soc. Am.,* **102**(5), 2239–2244.

Hollander, M. & Wolfe, D.A., 1973. *Nonparametric Statistical Methods,* John Wiley.

Julian, B., Miller, A.D. & Foulger, G.R., 1998. Non-double-couple earthquakes 1. Theory, *Rev. Geophys.,* **36**(4), 525–549.

Kawakatsu, H., 1991. Insignificant isotropic component in the moment tensor of deep earthquakes, *Nature,* **351,** 50–53.

Kawakatsu, H., 1996. Observability of the isotropic component of a moment tensor, *Geophys. J. Int.,* **126**(2), 525–544.

Kuge, K. & Lay, T., 1994. Data-dependent non-double-couple components of shallow earthquake source mechanisms: effects of waveform inversion instability, *Geophys. Res. Lett.,* **21**(1), 9–12.

Kwiatek, G. & Ben-Zion, Y., 2013. Assessment of P and S wave energy radiated from very small shear-tensile seismic events in a deep South Africa mine, *J. geophys. Res.,* **118,** 3630–3641.

Lewis, M., Peng, Z., Ben-Zion, Y. & Vernon, F., 2005. Shallow seismic trapping structure in the San Jacinto fault zone near Anza, California, *Geophys. J. Int.,* **162**(3), 867–881.

Lockner, D., Walsh, J. & Byerlee, J., 1977. Changes in seismic velocity and attenuation during deformation of granite, *J. geophys. Res.,* **82,** 5374–5378.

Ma, K., Lin, Y., Lee, S., Mori, J. & Brodsky, E.E., 2012. Isotropic events observed with a borehole array in the Chelungpu Fault Zone, Taiwan, *Science,* **337,** 459–463.

Minson, S.E., Dreger, D.S., Bürgmann, R., Kanamori, H. & Larson, K.M., 2007. Seismically and geodetically determined nondouble-couple source mechanisms from the 2000 Miyakejima volcanic earthquake swarm, *J. geophys. Res.,* **112,** B10308, doi:10.1029/2006JB004847.

Mitchell, T.M., Ben-Zion, Y. & Shimamoto, T., 2011. Pulverized fault rocks and damage asymmetry along the Arima-Takatsuki Tectonic Line, Japan, *Earth planet. Sci. Lett.,* **308,** 284–297.

Patton, H.J. & Taylor, S.R., 2011. The apparent explosion moment: Inferences of volumetric moment due to source medium damage by underground nuclear explosions, *J. geophys. Res.,* **116,** B03310, doi:10.1029/2010JB007937.

Pearce, R.G. & Rogers, R.M., 1989. Determination of earthquake moment tensors from teleseismic relative amplitude observations, *J. geophys. Res.,* **94**(B1), 775–786.

Reid, H., 1910. The mechanics of the earthquake, Vol. II, The California Earthquake of April 18, 1906, Report of the State Earthquake Investigation Commission, Carnegie Inst, *Wash. Publ,* 87.

Ross, Z.E. & Ben-Zion, Y., 2013. Spatio-temporal variations of double-couple aftershock mechanisms and possible volumetric earthquake strain, *J. geophys. Res.,* **118,** 2347–2355.

Stanchits, S., Vinciguerra, S. & Dresen, G., 2006. Ultrasonic velocities, acoustic emission characteristics and crack damage of basalt and granite, *Pure appl. Geophys.,* **163,** 975–994.

Tape, W. & Tape, C., 2013. The classical model for moment tensors, *Geophys. J. Int.,* **195,** 1701–1720.

Vavryčuk, V., 2014. Moment tensor decompositions revisited, *J. Seismol.,* **18**(4), doi:10.1007/s10950-014-9463-y.

Walter, W.R., Mayeda, K. & Patton, H., 1995. Phase and spectral ratio discrimination between NTS earthquakes and explosions, Part I: empirical Observations, *Bull. seism. Soc. Am.,* **85,** 1050–1067.

Wechsler, N., Rockwell, T.K. & Ben-Zion, Y., 2009. Application of high resolution DEM data to detect rock damage from geomorphic signals along the central San Jacinto Fault, *Geomorphology,* **113,** 82–96.

Yang, H., Zhu, L. & Cochran, E., 2011. Seismic structures of the Calico fault zone inferred from local earthquake travel time modeling, *Geophys. J. Int.,* **186,** 760–770.

Yang, W., Hauksson, E. & Shearer, P., 2012. Computing a large refined catalog of focal mechanisms for Southern California (1981–2010): temporal stability of the style of faulting, *Bull. seism. Soc. Am.,* **102**(3), 1179–1194.

Xu, H., Rodgers, A.J., Lomov, I.N. & Vorobiev, O.Y., 2012. Seismic source characteristics of nuclear and chemical explosions in granite from hydrodynamic simulations, *Pure appl. Geophys.,* **171,** 507–521.

Zhao, L. & Helmberger, D.V., 1994. Source estimation from broadband regional seismograms, *Bull. seism. Soc. Am.,* **84**(1), 91–104.

Zhu, L. & Ben-Zion, Y., 2013. Parameterization of general seismic potency and moment tensors for source inversion of seismic waveform data, *Geophys. J. Int.,* **194,** 839–843.

Zhu, L. & Helmberger, D.V., 1996. Advancement in source estimation techniques using broadband regional seismograms, *Bull. seism. Soc. Am.,* **86**(5), 1634–1641.

Zhu, L. & Rivera, L., 2002. A note on the dynamic and static displacements from a point source in multi-layered media, *Geophys. J. Int.,* **148,** 619–627.

Zigone, D., Ben-Zion, Y., Campillo, M. & Roux, P., 2015. Seismic tomography of the Southern California plate boundary region from noise-based Rayleigh and Love waves, *Pure appl. Geophys.,* **172**(3), doi:10.1007/s00024-014-0872-1.